Nanoscale Advances

ROYAL SOCIETY OF CHEMISTRY

COMMUNICATION

View Article Online
View Journal | View Issue



Cite this: *Nanoscale Adv.*, 2020, **2**, 3821

Received 9th May 2020
Accepted 7th July 2020

DOI: 10.1039/d0na00377h

rsc.li/nanoscale-advances

# Fractal structures and silica films formed by the Treignac water on inert and biological surfaces†

Agnès Smith, *[a] Fatima Zahra Abir,[a] Youssef El Hafiane,[a] Yann Launay,[a] Céline Faugeron-Girard,[b] Vincent Gloaguen,[b] Thierry Devers,[c] Anaïs Raynaud,[d] Charlotte Moine,[d] Jean Sainte-Laudy,[e] Thibaud Latour,[f] Jean-Francois Hausman[g] and Gea Guerriero [g]

The Treignac water is a natural mineral water containing mainly orthosilicic acid. On inert substrates, it forms a silica film with fractal structures which cannot be reproduced in laboratory-reconstituted water. These structures form by condensation of orthosilicic acid monomers, following the Witten–Sander model of diffusion-limited aggregation. On biological surfaces, such as tomato leaves, the Treignac water forms a silica film with a different morphology and devoid of fractal structures. The filmogenic properties of this natural mineral water are here discussed in the context of crop protection, as the silica film can provide a barrier and a platform for the immobilization of elicitors of plant defense responses.

## 1 Introduction

Silicon is the second most abundant element on Earth after oxygen and is an important trace element in the human body, contributing to the health of bones, connective tissue, as well as skin, nails and hair.[1] Silicon is released from the Earth's crust as orthosilicic acid ($Si(OH)_4$) through rainfall and it is essentially inert in under-saturating conditions (below 2 mmol $L^{-1}$).[2] Beyond this concentration, it spontaneously precipitates as amorphous silica ($SiO_2$). Orthosilicic acid has a unique inorganic chemistry with aluminium hydroxide: through competitive substitution, hydroxyaluminosilicates form,[2–4] which contribute to keep aluminium out of biota.[2] Recent research has additionally shown that silicon favours the excretion of aluminium from the body.[5–7]

Drinking water contains readily bioavailable sources of silicon for humans.[8] The Treignac water is a natural mineral water from a small village located in the Corrèze mountains in Limousin (France) with a low mineral content, containing mainly orthosilicic acid. Historically known by the pilgrims on the route to St James of Compostella because of its skin soothing properties, this water, both natural and concentrated,[9] forms a silica film containing previously-reported fractal structures (fractal dendrites) on inert metallic substrates.[10] The filmogenic properties and orthosilicic acid content of the Treignac mineral water are already used in cosmetics because of the clinically-proven moisturizing and protective effects.[10] However, no study has yet been undertaken to analyse how these structures form. Likewise, the composition of these forms and the eventual interferences of the physico-chemical environment on their formation have not yet been investigated.

By combining transmission (TEM), simulations and environmental scanning electron microscopy (SEM) coupled to energy dispersive spectroscopy (EDS), we here show that the dendrites and fractal structures derive from the polymerisation of orthosilicic acid by condensation of monomers, according to the Witten–Sander model of diffusion-limited aggregation (DLA).[11] Notably, the fractal dendrites cannot be reproduced when laboratory-reconstituted water containing exactly the same amounts of elements and pH as the Treignac water is deposited on an inert surface. Additionally, a film devoid of any fractal structure forms when the water is deposited on biological surfaces, such as the leaf of tomato plants.

Besides cosmetics, the Treignac water's filmogenic properties have interesting applications in other fields, namely as a coating agent for crop protection. We discuss the potential

[a]*Institut de Recherche sur les Céramiques, CNRS UMR 7315, Université de Limoges, Centre Européen de la Céramique, 12 rue Atlantis, 87068 Limoges cedex, France. E-mail: agnes.smith@unilim.fr*

[b]*Laboratoire Peirene, EA 7500, Université de Limoges, 123 Avenue Albert Thomas, 87060 Limoges cedex, France*

[c]*Interfaces, Confinement, Matériaux et Nanostructures, CNRS UMR 7374, IUT de Chartres, Université d'Orléans, 1 bis rue de la Férollerie, CS 40059, 45071 Orléans cedex, France*

[d]*Covertis, Ester Technopole, 1 avenue d'Ester, 87069 Limoges Cedex, France*

[e]*Société des eaux de Source de Treignac (SEST), Le Borzeix, 19260 Treignac, France*

[f]*IT for Innovative Services–Human Dynamics in Cognitive Environments, Luxembourg Institute of Science and Technology, 5 avenue des Hauts-Fourneaux, L-4362 Esch/Alzette, Luxembourg*

[g]*Environmental Research and Innovation Department, Luxembourg Institute of Science and Technology, 5, rue Bommel, Z. A. E. Robert Steichen, L-4940, Hautcharage, Luxembourg*

† Electronic supplementary information (ESI) available. See DOI: 10.1039/d0na00377h

uses of the film to immobilize elicitors of plant defense responses.

# 2 Experimental

## 2.1 Sample preparation

The samples studied in this work are the following:

(a) The natural mineral water (hereafter referred to as TN).

(b) The concentrated water prepared by inverse osmosis (hereafter referred to as TO) and obtained by filtration on a polyamide membrane (CSM ref RE-2540-TE) until a concentration ratio of 10 was reached.[9] This method allows to keep the same mineral equilibrium for both TN and TO.

(c) A dry powder (hereafter referred to as DP): TN was lyophilized (ODESSOL laboratory, University of Limoges, France) on the basis of preliminary studies having shown that the mineral residue was totally soluble in water. A bench freeze dryer CRYOTECH Cosmo 80 was used, with the following parameters: pressure <50 mTorr, temperature −80 °C, isobar temperature rising up to 20 °C in 36 h. Samples were frozen in liquid nitrogen, stabilized at −80 °C and placed in the freeze dryer. Vials were immediately closed and kept at 4 °C.

## 2.2 Chemical analyses

The chemical composition of the water was determined by Inductively Coupled Plasma-Atomic Emission Spectroscopy (ICP-AES, PerkinElmer, Optima 8300 DV). Anion assays were performed in a reference laboratory (Veterinary laboratory, Tulle, France) according to standardized methods (NF EN ISO 10304-1 for $Cl^-$, $SO_4^{2-}$ and $NO_3^-$ and NF EN ISO 9963-1 for $SO_4^{2-}$). The dry residue obtained at 180 °C was measured by the ISO NF T90-029 method.

## 2.3 Electron microscopy

In order to study the morphology of the mineral parts contained in the different samples, two different techniques were used, namely environmental Scanning Electron Microscopy, SEM (FEI, QUANTA FEG 450) equipped with an Energy Dispersive Spectroscopy, EDS, system (SAM'X) and Transmission Electron Microscopy, TEM (JEOL, JEM-2100F) equipped with an Energy Dispersive Spectroscopy system (JEOL, vEX-24063JGT). For SEM, a metallic substrate was first carefully cleaned with deionized water and dried with clean air. Then, a carbon film was glued onto the sample. A drop of water was deposited on the substrate and dried under a lamp for a few minutes. The sample was immediately introduced in the SEM chamber to avoid any deposition of dust. For TEM, a copper grid (diameter: 3 mm) coated with a carbon membrane was deposited on a glass substrate. A drop of water was deposited on the grid, dried and immediately introduced in the TEM chamber.

Tomato plantlets (var. Marmande) were obtained four weeks after sowing in a greenhouse. The Treignac water was applied on the leaf surface following three different protocols. For the first one, plantlets were sprayed with TO until run-off every day for three days. On day four, they were harvested and immediately frozen in liquid nitrogen before SEM analysis. The second protocol consisted in cutting a small piece of leaf and applying 5 μL of TO on it just before analysing with SEM. For the third one, 5 μL of TN or TO were deposited on the leaf surface under greenhouse conditions (22 °C, 60% humidity) and left to evaporate during one hour. SEM analysis was performed the day after.

In order to study the behaviour of the Treignac water on a hydrophobic surface, a 2 μL-drop of TN was deposited on a mimosa wax tablet and immediately introduced in the SEM chamber.

## 2.4 X-ray powder diffraction, thermogravimetric analysis-differential thermal analysis

X-Ray diffraction (XRD) data were acquired at room temperature on a Bruker D8 Advance X-ray diffractometer with $CuK_\alpha$ radiation ($\lambda_{Cu} = 1.54056$ Å) at a step scan of 0.01 at a voltage of 40 kV with an electric current of 40 mA. Phase identification was carried out using the EVA program. Differential scanning calorimetry (DSC) was performed on two samples with the same weight in order to compare the signal intensity. The DSC scans were taken with a Thermo-balance TG-DSC Setsys Setaram 24 apparatus. The firing cycle was the following: heating ramp 5 °C $min^{-1}$ up to 1200 °C, dwell time 1 hour, cooling ramp 5 °C $min^{-1}$.

## 2.5. Computer simulation

A simulation of the DLA process was implemented. The simulation starts with a random uniform distribution of particles represented by single pixels on a 2D regular grid and lets them, at each simulation cycle, make one grid unit translations towards any of the eight neighbouring positions or 90° left or right rotations around a randomly selected centre among the aggregate monomers, until they collide with another particle or aggregate and stick to it. Aggregates hence created are free to continue moving and rotating randomly and be further aggregated until all particles form a single structure or until a maximum number of simulation steps has been reached. In order to account for evaporation, at every simulation step, a fraction of available positions for aggregate movement are randomly selected and removed until complete elimination. Such removal progressively limits the aggregate movements.

A series of 4 simulations was performed by combining orthosilicic acid concentrations in TN and TO water and the effect of evaporation on a flat surface. The 2D grid size was set to 320 × 240 pixels on the grid. The particle fraction was estimated as the molar fraction of the Si content of TN (6.6 mg $L^{-1}$) and water solvent, further multiplied by $10^3$ to keep the simulation time relatively short. Hence, TN particle fraction was set to 0.00198 (yielding about 150 monomers) and TO particle fraction was set to 0.0198 (yielding about 1500 monomers). To evaluate the possible effect of the solvent evaporation on the process, the fraction of removed available grid points for particle and aggregate movements at every simulation step was set to 0.0005, wherever evaporation was considered. The maximum number of simulation steps was set to 5000.

 

# 3 Results and discussion

## 3.1 Chemical composition of the Treignac water samples

Table 1 shows the elemental composition of the different water samples analysed. The mineral content in TN is low compared to most mineral waters.[12–17] Orthosilicic acid (hereafter referred to as "silica", as often done when describing the composition of natural mineral water) represents 33% of the dry residue. Its pH is equal to 5.8. In TO, the quantity of each element is approximately ten-times higher as compared to TN and the percentage of orthosilicic acid is maintained at 33%.

Table 1 Chemical composition (in mg $L^{-1}$) of the natural Treignac water (TN) and the Treignac water after osmosis (TO). The percentage of orthosilicic acid is 33% in both TN and TO

| Element | Content in TN (mg $L^{-1}$) | Content in TO (mg $L^{-1}$) |
|---|---|---|
| $Ca^{2+}$ | 1.20 | 11.70 |
| $Mg^{2+}$ | <0.5 | 3.70 |
| $Na^{+}$ | 2.80 | 24.40 |
| $K^{+}$ | <0.5 | 2.80 |
| $SiO_2$ | 6.60 | 62.30 |
| $Cl^{-}$ | 3.20 | 27.00 |
| $NO_3^{-}$ | 3 | 26.00 |
| $SO_4^{2-}$ | <1 | 5.23 |
| Residue after thermal treatment at 180 °C | 20 | 190.33 |

## 3.2 High resolution imaging of the Treignac water samples and elemental composition of the fractal structures

The images at the SEM show the typical morphologies observed for the mineral parts contained in TN (Fig. 1A) and TO (Fig. 1B). They present films with fractal dendrites. In some places, cubic crystals are seen on the surface (Fig. 1B).

TEM observations and EDS analysis on TN show that the mineral parts consist of an aggregation of small particles (Fig. 2A) of silicon and oxygen (Fig. 2B). The elemental analysis was performed on different regions of the aggregates and the result was highly reproducible and equivalent to Fig. 2B.

## 3.3 Model explaining the formation of the fractal structures in the Treignac water samples

In order to explain the formation of the fractal structures, one should refer to Brinker's article describing the sol–gel processing of silica from organometallic precursors in an organic

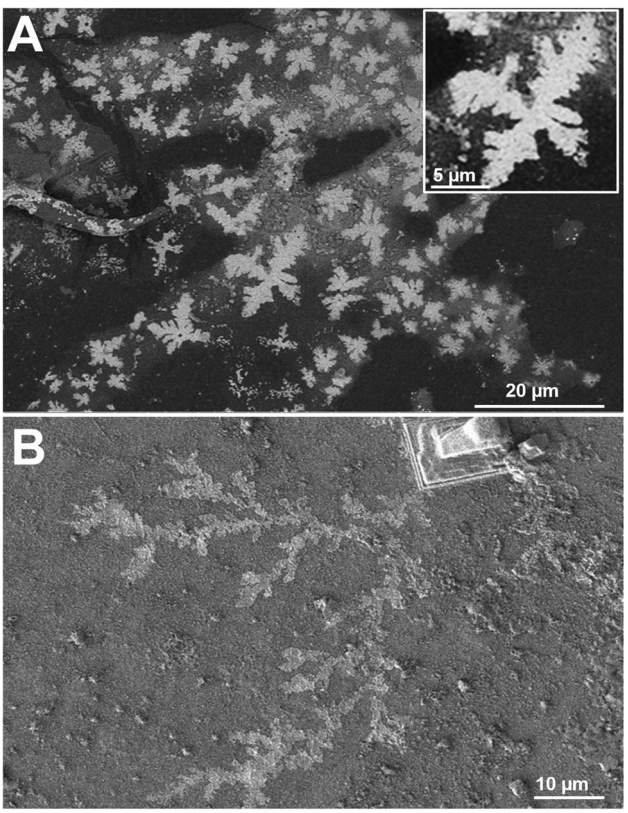


Fig. 1 SEM analysis revealing the typical morphologies of the mineral parts contained in (A) TN, and (B) TO waters. Inset in A: magnification of fractal dendrite in TN, showing the typical self-similarity of fractal structures.

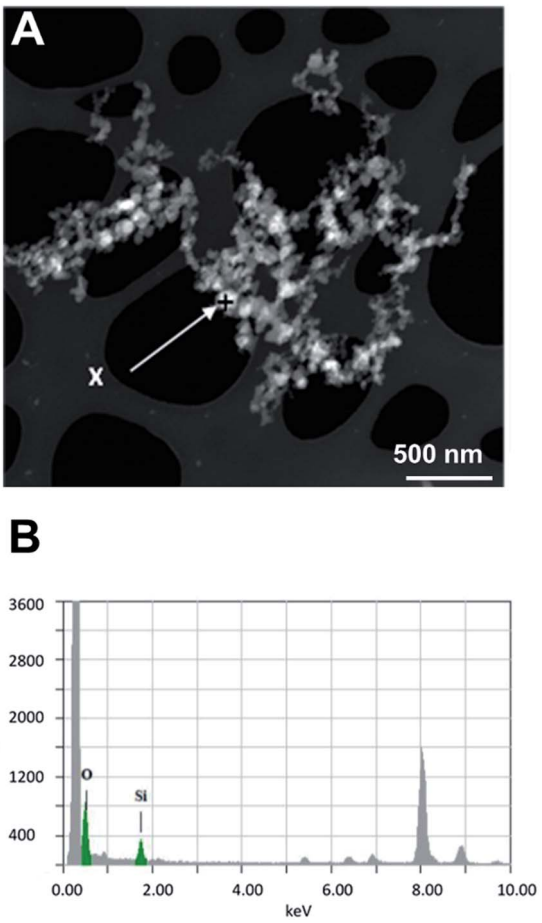


Fig. 2 TEM and EDS analyses of TN. (A) TEM observation of TN showing the aggregation of small particles. (B) EDS analysis on the surface (region indicated with the letter "X"). The grey peaks correspond to the copper grid on which TN was deposited.

solvent.[18] What is very different in the present study is the absence of organometallic silica precursors and the organic solvent. Nevertheless, the chemical mechanisms described by Brinker[18] apply to the Treignac water samples. In this water, orthosilicic acid can form a dimer which, as previously described for the condensation reaction,[19] further polymerizes into linear and cyclic structures, oligomers, particles and finally aggregates, whose conformation and length depend on the pH and the ionic content of the solution. The fractal dendrites observed more frequently in TO (Fig. 1) are characteristic of the condensation of monomers with growing clusters and with a diffusion-limited growth.[11,20] In this model, the monomer moves randomly in the solution (Brownian motion) and as soon as it meets the cluster, it sticks to it. The monomer does not have time to diffuse within the growing cluster and the resulting polymer thus shows dendrites.

Evaporation is predicted to influence the aggregates' sizes and distribution (Fig. 3). The rapidity of evaporation is also known to affect the formation of ordered patterns: rapid evaporation promotes the formation of fingering patterns by convective forces.[21] The results of the simulation show systematic larger and more compact aggregates (as shown by the average number of neighbours per monomer and the radial distribution function in Fig. 4) with the more concentrated TO water (Fig. 3C and D and Videos in ESI†), irrespective of evaporation. By progressively lowering the freedom of movement of the particles and aggregates, evaporation also results in the growth of smaller and more distributed aggregates with a distribution that is affected by the spatial non-uniformity of the evaporation probability that we introduced in the simulation (Fig. 3B and D).

These preliminary simulations are in rather good agreement with the observations made (Fig. 1 and 2) and constitute a first step in rationalising them. Yet, several limitations are still present. Indeed, even if modifying the random walk of particles and aggregates in the DLA simulation with a basic representation of evaporation tends to reproduce the experimental observations, it says nothing about the underlying physical and chemical processes involved. Several aspects are worth further investigations, such as the use of a three dimensional water model with precipitation, the analysis of the morphology of 3D aggregates and their 2D projections on the surface.

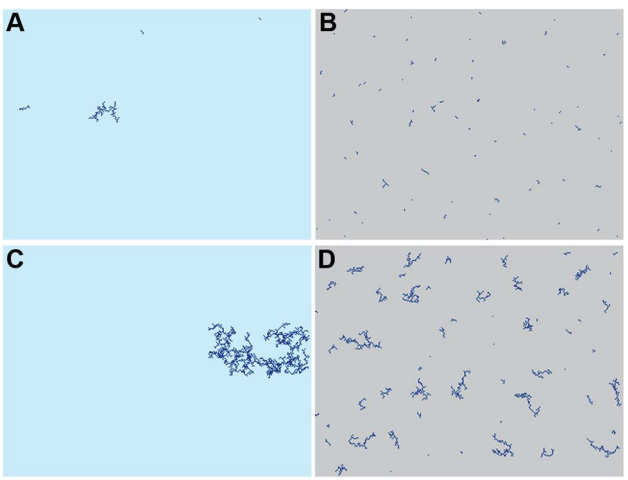


Fig. 3 Computer simulations of the DLA process applied to the Treignac water. Final states without evaporation on a flat surface for TN (A) and TO (C). Computer simulations of the final states with evaporation on a flat surface for TN (B) and TO (D).

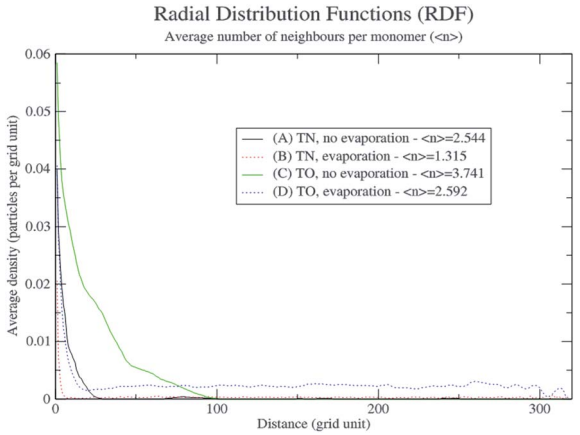


Fig. 4 Radial distribution functions and average number of neighbours per monomer of the DLA process applied to TN and TO.

### 3.4 Structural analyses and thermal characterisation

XRD on DP presents one crystalline phase, NaCl (Fig. 5), which corresponds to the large cubic crystals shown in Fig. 1B. No crystalline peak corresponding to $SiO_2$ is recorded by XRD, which means that silica is amorphous.

Thermogravimetric analysis-differential thermal analysis (TGA-DTA) on DP is recorded under air (Fig. 6A) and nitrogen atmosphere (Fig. 6B). Under air, two peaks are present at low temperature: an endothermic peak around 100 °C (1), related to the evaporation of water contained in the lyophilized powder, followed by a second endothermic peak (2), around 120 °C, probably corresponding to the loss of the remaining water that is strongly bound to DP. The complete dehydration of DP corresponds to a mass loss of 18%. Under nitrogen atmosphere, a large peak is recorded and corresponds to a mass loss of 6%.

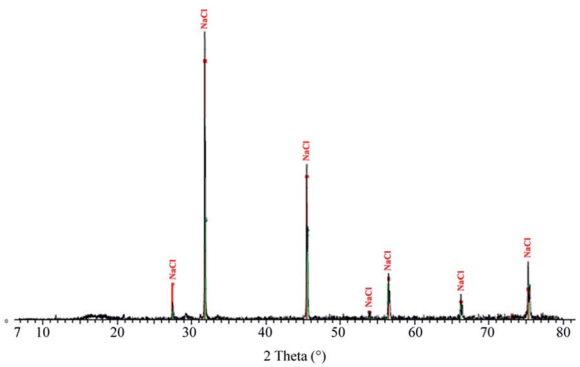


Fig. 5 XRD analysis on TO showing the presence of crystalline NaCl.

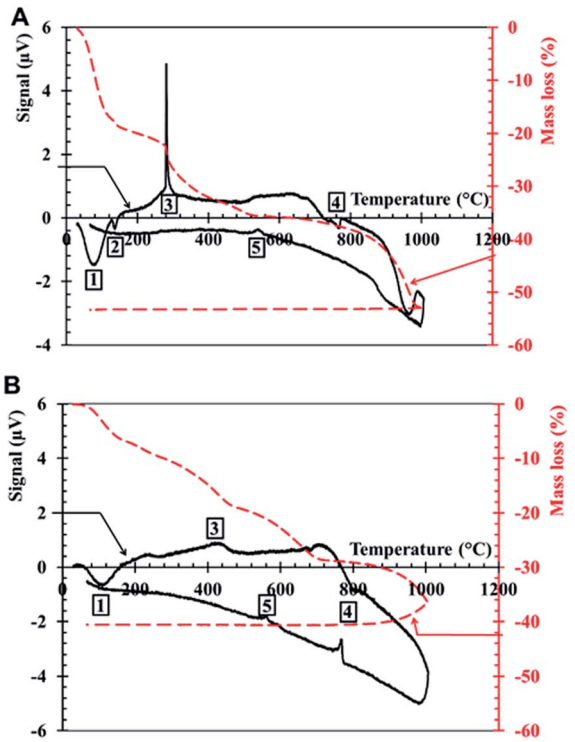


Fig. 6 TGA-DTA analysis on DP under air (A) and under nitrogen (B).

An exothermic peak is measured in air at 300 °C (3), while there is no peak under nitrogen. This peak likely corresponds to the combustion and the decomposition of organic matter in air. During its underground travel, the Treignac water may collect tiny quantities of organic matter, such as humic-like substances (HS) which are polymeric chains. According to the composition of the forest, the soil of the impluvium and the presence of traces of organic carbon, it is reasonable that the Treignac water contains HS. The HS content in the water is too small to be detected, but it can be concentrated in the DP, after the lyophilisation process. The thermal decomposition of HS can occur in a large temperature range, up to 500–600 °C.[22] According to TGA, the mass loss at 300 °C is of a few percent. HS decomposition could contribute to this mass loss.

An endothermal peak is present around 780 °C (4) in air and 800 °C under nitrogen atmosphere and it is due to the fusion of NaCl.

During cooling, the exothermic peak at 573 °C (5) corresponds to the well-known polymorphic transformation between quartz β and quartz α.

The total mass loss during heating between room temperature and 1000 °C is equal to 53% under air and 41% under nitrogen. This variation is mainly due to the difference between the water loss under air and under nitrogen atmosphere.

### 3.5 Analysis of a laboratory-reconstituted water mimicking TN

In order to understand if the pH and/or the ionic content of the water are responsible for the development of the fractal morphologies, we used pure grade atomic spectroscopy calibration standards and mixed them in order to reproduce as closely as possible the ionic cocktail contained in the natural Treignac water. The different reference solutions are presented in Table 2. They all contain small amounts of acids, mostly nitric acid and hydrofluoric acid (for the silicon standard), necessary to maintain the elements dissolved in solution. Concerning the supply of chloride, NaCl was added so that the concentration of $Cl^-$ is similar to its value in TN.

Table 2 Pure grade standards used for the reconstitution of the Treignac water. The reference numbers of the supplier (Perkin Elmer) are also provided

| Chemical element (1000 mg $L^{-1}$) | Matrix | Product reference (supplier: PerkinElmer) |
|---|---|---|
| $Ca^{2+}$ | $H_2O$ with 2% $HNO_3$ | Calcium pure single-element standard (Ref.: N9303763) |
| $Mg^{2+}$ | $H_2O$ with 2% $HNO_3$ | Magnesium pure single-element standard (Ref.: N9300179) |
| $Na^+$ | $H_2O$ with 2% $HNO_3$ | Sodium pure single-element standard (Ref.: N9303785) |
| $K^+$ | $H_2O$ with 2% $HNO_3$ | Potassium pure single-element standard (Ref.: N9303779) |
| Si | $H_2O$ with traces of HF | Silicon pure single-element standard (Ref.: N9303799) |

To understand whether the ionic content or the pH or both are implicated in the formation of the fractal objects, two experimental strategies were designed, as explained below:

(a) A water containing exactly the same amounts of elements as in TN was reconstituted. This water is called TE (E for element). The main difference with TN was the pH, since it was equal to 2.9 due to the presence of nitric and hydrofluoric acids in very small quantities.

(b) A water that has the same ionic content and pH as TN, *i.e.* 5.8, was reconstituted. For this purpose, we increased the pH of TE by adding a small amount of NaOH. This water is called TpH and it contains more sodium ions (24 mg $L^{-1}$) than TN (2.8 mg $L^{-1}$).

Fig. 7 shows the morphologies obtained for TE and TpH. With TE (Fig. 7A), small beads are formed. They are characteristic of a growth limited by a cluster–cluster reaction (Brinker, 1988). This model is described for pH < 3, when the condensation rate of aqueous silica is low since they are not ionised.[23] In this mechanism, the monomers have a Brownian motion and stick to other monomers to form clusters. The final object is poorly ramified. With TpH, the morphology consists of large spheres (Fig. 7B) that can form at pH close to neutrality.[24] The aggregation of the individual monomers is very fast and can be responsible for the formation of spheres,[23] thus minimizing the surface energy. TpH has a higher pH than TE and it is known that at higher pH condensation reactions are faster.[25]

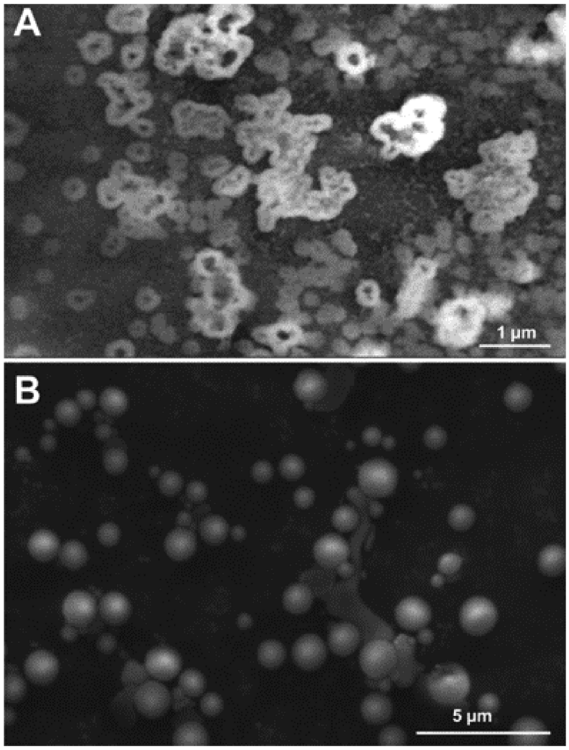


Fig. 7 Morphology of TE (A) and TpH (B).

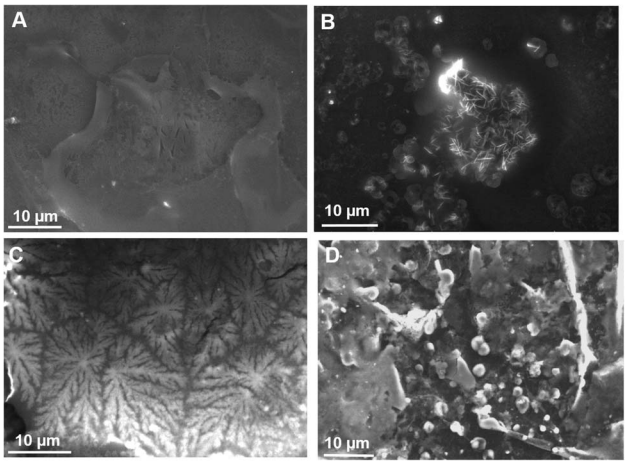


Fig. 8 Environmental scanning electron microscopy images of the structures formed by TN and TpH on the surface of a tomato leaf or on the flat surface of a wax tablet previously chilled at 4 °C. (A) Surface of a tomato leaf where a drop of TN was deposited, left to evaporate and observed under high humidity (98.7%). (B) Surface of a tomato where a drop of TpH was deposited, left to evaporate and observed under high humidity (98.8%). (C) Details of the thin TN film showing fractal dendrites on the flat surface of the pre-chilled wax tablet (observations under 84.6% humidity). (D) Details of the round objects formed by a drop of TpH on the flat surface of the pre-chilled wax tablet (observations under 99.4% humidity).

The results obtained (Fig. 7) show that salt content and pH strongly impact the morphology of the aggregates. The probability introduced in the DLA seminal paper[11] that a particle will adhere to the cluster aggregate when in contact with it was not introduced in the simulation. If we hypothesise that pH and salt content influence the monomer reactivity, it is possible to reasonably represent such modified reactivity with varying adherence probabilities. Since smaller sticking coefficients in DLA simulations tend to produce more compact aggregates by letting particles penetrate more deeply into the dendritic structure before polymerizing, such effect may be crucial to rationalise the experimental observations.

### 3.6 High resolution imaging of the Treignac water samples on the surface of a leaf

Observations of the film formed by the TN were carried out on biological surfaces, namely the leaf of a tomato plant. The rationale was to study whether fractal objects form on the leaves of an important crop and provide a moisturizing barrier which could mitigate the adverse effects of abiotic stresses, such as drought/salt stress. Fractal geometries also possess a high surface area and are thus ideal for functionalization of coatings,[26] *e.g. via* the immobilization of elicitors of plant defense responses.

TN deposited on tomato leaves did not result in any fractal structure (Fig. 8A), while TpH resulted in the appearance of needle-like objects arranged in druses (Fig. 8B). A complementary SEM analysis was performed on wax tablets mimicking a hydrophobic surface like that of leaves. TN was deposited and evaporated under SEM conditions. Dendrites appeared (Fig. 8C) that were equivalent to those already observed on a metallic surface (Fig. 1). The flatness of the surface seemed, however, to be a determining factor for the formation of dendrites, since the deposition of TN on the curved surface of a wax tablet left a film with no dendrites (not shown). TpH deposited on the flat surface of a wax tablet resulted in the formation of spherical objects (Fig. 8D), like those observed on a metallic surface (Fig. 7B).

Tomato plants sprayed with TO show the presence of a film covering the epidermal cells and replicating their corrugated surfaces (Fig. S1B†). Such a film is absent on leaves sprayed with demineralised water (Fig. S1A†). When the humidity is lowered from *ca.* 100% to 50%, cracks become visible on the surface of treated leaves (Fig. S1C†) and they become very clear at 0% (Fig. S1D†). In some images, it is possible to see a layer of the film peeling off from the leaf surface (Fig. S1D inset†). The thickness of the film is estimated to be *ca.* 100 nm.

In order to follow the formation of the silica film in real-time, a drop of TO was deposited on the surface of a tomato leaf (Fig. S1E†) and the sample was then immediately placed in the chamber for observation. Over time, a film forms (Fig. S1F†). The EDS analysis confirms the presence of silicon in the film forming on the treated surface, while no silicon signal is present on the region immediately adjacent to the treated area (Fig. 9).

Observations were also performed on the surface of leaves on which a drop of TO was deposited and left to evaporate under greenhouse conditions. A clear layer forms on the treated leaves (Fig. S1H†), with the sporadic presence of flakes (Fig. S1H,

 

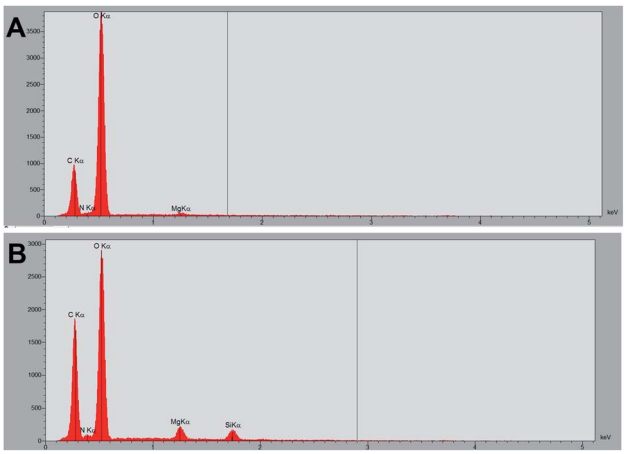


Fig. 9 Energy dispersive spectroscopy carried out on the surface of a tomato leaf. (A) untreated (reference) region. (B) treated region on which a drop of TO was deposited and immediately observed at the electron microscope.

inset†). The surface of control leaves appears instead devoid of any film (Fig. S1G†).

TO was deposited and evaporated under SEM conditions. A thin film formed after evaporation (Fig. S1I†) and fractal dendrites appeared (Fig. S1J†).

## 4 Conclusions

We confirm here that the Treignac mineral water, natural or concentrated by reverse osmosis, is capable of generating a film constituted of fractal structures, *i.e.* fractal dendrites. The simulations predict that the concentrated water (TO) forms bigger aggregates, as observed in reality on flat metallic and wax surfaces. Such fractal objects are characteristic of the condensation of monomers of orthosilic acid with growing clusters and with a diffusion-limited growth. We have shown that these fractal forms are composed of condensed silicic acid, that their formation is sensitive to the physico-chemical environment and, in particular, to salt content and pH. Concerning the factors responsible for the morphology, neither the ionic content nor the pH could explain it. Further investigations are currently in progress in order to validate other hypotheses based on other eventual physical and/or chemical mechanisms taking place during the infiltration of rain water through the soil and subsoil and during the underground trip of the water in the granitic/metamorphic massif of Limousin. The presence of organic substances like HS, even in small quantities, could indeed play a role in the growth of such fractal objects. Impurities may fix the aggregates, thus contributing to create small "islands" which should distribute according to the impurity locations.

On biological surfaces, such as the leaf of tomato plants, a film forms, but it is devoid of any fractal objects. Under reduced humidity, the film cracks and peels off from the leaf surface. The flatness of the surface is important to let the dendrites form. The presence of trichomes (leaf hair) on the leaf surface and the corrugated surface of the epidermal cells could interfere with the formation of dendrites. Future simulations taking into account the surface topology, as well as the presence of impurities can confirm that the topology of the surface plays a role in the distribution of the aggregates.

The filmogenic properties of TN and TO can be used to coat the leaves of crops with a silica film. The coating can increase the plant resistance to pathogens *via* a dual mechanism, *i.e.* a barrier and a biological effect due to the presence of orthosilicic acid. In addition to these mechanisms, there is also a synergistic effect provided by the immobilization of elicitors of plant defense responses on the film: this type of film functionalization improves the persistence of the elicitor, thereby intensifying the protective effect.

## Author contributions

A. S., F. Z. A., Y. E. H., Y. L., C. F.-G., V. G., T. D., A. R., C. M., J. S.-L., J.-F. H. and G. G. contributed to writing, SEM experiment planning on biological surfaces and wax tablets and participated to data interpretation. TL performed all the simulations and interpreted the results.

## Conflicts of interest

J. S.-L. is consultant for the Société des Eaux de Source de Treignac. A. R. is a scientist working at COVERTIS, a company developing products through green chemistry and used in phytoprotection. CM is CEO and founder of COVERTIS.

## Acknowledgements

This project has benefited from the financial support of the Région Nouvelle-Aquitaine and the Banque Publique d'Investissement (France). Characterization data were performed using the CarMaLim platform in the CERamics Research Institute, Limoges, France.

## References

1 L. A. de Araújo, F. Addor and P. M. B. G. M. Campos, *An. Bras. Dermatol.*, 2016, **91**, 331–335.
2 C. Exley, G. Guerriero and X. Lopez, *Sci. Total Environ.*, 2019, **665**, 432–437.
3 C. Exley, *Coord. Chem. Rev.*, 2012, **256**, 82–88.
4 J. Beardmore, X. Lopez, J. I. Mujika and C. Exley, *Sci. Rep.*, 2016, **6**, 30913.
5 D. Dobrzyński and C. Exley, *Acta Balneologica*, 2010, **52**, 296–304.
6 S. Davenward, P. Bentham, J. Wright, P. Crome, D. Job, A. Polwart and C. Exley, *J. Alzheimer's Dis.*, 2013, **33**, 423–430.
7 K. Jones, C. Linhart, C. Hawkins and C. Exley, *EBioMedicine*, 2017, **26**, 60–67.
8 R. Jugdaohsingh, S. H. Anderson, K. L. Tucker, H. Elliott, D. P. Kiel, R. P. Thompson and J. J. Powell, *Am. J. Clin. Nutr.*, 2002, **75**, 887–893.

9 World Intellectual Property Organization, WO2017162957A1, 2017.
10 J. Sainte-Laudy, G. Redziniak, A. Pons and T. Devers, A. Study by SEM of the filmogenic effect of mineral waters, *Particular case of the water of Treignac. 4e Workshop Expert'Labs*, Fuveau, June, 2016.
11 T. A. Witten and L. M. Sander, *Phys. Rev. B: Condens. Matter Mater. Phys.*, 1983, **27**, 5686–5697.
12 A. Versari, G. P. Parpinello and S. Galassi, *J. Food Compos. Anal.*, 2002, **15**, 251–264.
13 S. Giammarioli, M. Mosca and E. Sanzini, *J. Food Sci.*, 2005, **70**, s509–s512.
14 S. Platikanov, V. Garcia, I. Fonseca, E. Rullán, R. Devesa and R. Tauler, *Water Res.*, 2013, **47**, 693–704.
15 V. Lekskulchai, *Sci. Asia*, 2015, **41**, 409.
16 D. T. Udagedara and D. T. Jayawardana, *J. Earth Sci. Environ.*, 2015, **73**, 7957–7965.
17 C. C. Lesaulnier, C. W. Herbold, C. Pelikan, D. Berry, C. Gérard, X. Le Coz, S. Gagnot, J. Niggemann, T. Dittmar, G. A. Singer and A. Loy, *Microbiome*, 2017, **5**, 126.
18 C. J. Brinker, *J. Non-Cryst. Solids*, 1988, **100**, 31–50.
19 D. J. Belton, O. Deschaume and C. C. Perry, *FEBS J.*, 2012, **279**, 1710–1720.
20 D. W. Schaefer, *MRS Bull.*, 1988, **13**, 22–27.
21 M. Byun and Z. Lin, in *Evaporative Self-Assembly of Ordered Complex Structures*, World Scientific, 2011, pp. 295–349.
22 C. Martias, N. Villandier, E. Thune, A. Glomot, V. Gloaguen and A. Smith, *Appl. Clay Sci.*, 2015, **114**, 609–616.
23 C. Brinker and G. Scherer, *Sol Gel Science: The Physics And Chemistry Of Sol Gel Processing*, Academic Press, 1990.
24 R. K. Iler, *The Chemistry of Silica: Solubility, Polymerization, Colloid and Surface Properties and Biochemistry of Silica*, John Wiley & Sons, 1979.
25 E. G. Vrieling, Q. Sun, T. P. M. Beelen, S. Hazelaar, W. W. C. Gieskes, R. A. van Santen and N. A. J. M. Sommerdijk, *J. Nanosci. Nanotechnol.*, 2005, **5**, 68–78.
26 S. Shin, M.-L. Gu, C.-Y. Yu, J. Jeon, E. Lee and T.-L. Choi, *J. Am. Chem. Soc.*, 2018, **140**, 475–482.

 